Effects of reaction progress variable definition on the Flame Surface Density transport statistics and closure for different combustion regimes

Vassilios Papapostolou[1], Nilanjan Chakraborty[1], Markus Klein[2*], Hong G. Im[3]

[1]School of Engineering
University of Newcastle
Claremont Road, Newcastle
NE1 7RU, UK
Email: V.S.Papapostolu1@ncl.ac.uk ; nilanjan.chakraborty@ncl.ac.uk

[2]Universität der Bundeswehr München, Fakultät für Luft- und Raumfahrttechnik, LRT1,
Werner-Heisenberg-Weg 39, 85577 Neubiberg, Germany
Email: markus.klein@unibw.de

[3]Clean Combustion Research Center,
King Abdullah University of Science and Technology (KAUST),
Thuwal 23955-6900, Saudi Arabia
Email: hong.im@kaust.edu.sa

[*] Corresponding author

ABSTRACT

The implications of the choice of reaction progress variable on the performances of the Flame Surface Density (FSD) based mean reaction rate closure and the well-established sub-models of the FSD transport have been analysed in context of Reynolds Averaged Navier Stokes simulations. For this purpose, a detailed chemistry Direct Numerical Simulation (DNS) database of freely-propagating H_2 −air flames (with an equivalence ratio of 0.7) spanning the corrugated flamelets, thin reaction zones and broken reaction zones regimes of premixed turbulent combustion has been considered. The FSD and the unclosed terms of its transport equation have been analysed for reaction progress variables defined based on normalised H_2, O_2 and H_2O mass fractions and temperature. The performances of the closures for turbulent flux of FSD, and tangential strain rate term have been found to be mostly unaffected by the choice of reaction progress variable. However, the well-established existing models for the unresolved tangential strain rate term have been found not to perform well for the cases representing the corrugated flamelets and thin reaction zones regimes of premixed combustion. The performance of a well-established existing model for the combined propagation and curvature terms has been found to be significantly dependent on the choice of reaction progress variable. Furthermore, the surface-averaged value of the density-weighted displacement speed cannot be approximated by the corresponding unstretched laminar flame value especially for the flames in the broken reaction zones regime. Detailed explanations have been provided for the observed behaviours of the FSD based reaction rate closure and sub-models for the unclosed terms of the FSD transport equation in different combustion regimes for different choices of reaction progress variable.

Keywords: Flame Surface Density, Reynolds Averaged Navier Stokes simulations, Reaction progress variable, Reaction rate closure, Direct Numerical Simulations

1. INTRODUCTION

The mean reaction rate closure in premixed turbulent combustion is often achieved using the flame surface density (FSD), defined as the flame surface area per unit volume (Candel and Poinsot, 1990). The generalised FSD is defined as (Boger *et al*., 1998): $\Sigma_{gen} = \overline{|\nabla c|}$ where c is the reaction progress variable (RPV) and the overbar indicates a Reynolds averaging or filtering operation in the context of Reynolds-averaged Navier-Stokes (RANS) or large eddy simulations (LES). A number of previous analyses focussed on both algebraic (Boger *et al*., 1998; Cant and Bray, 1998; Charlette *et al*., 2002; Knikker *et al*., 2002; Keppeler *et al*., 2014; Klein *et al*., 2016; Chakraborty and Klein., 2008a; Ma *et al*., 2013) and transport equation (Cant *et al.*, 1990; Candel *et al.*, 1990; Duclos *et al.*, 1993; Veynante *et al.*, 1996; Hawkes and Cant 2001a; Chakraborty and Cant, 2007; Hun and Huh, 2008; Katragadda *et al.*, 2011; Chakraborty *et al.*, 2011; Hernandez-Perez *et al.*, 2011; Reddy and Abraham, 2012; Chakraborty and Cant, 2013; Ma *et al.*, 2014; Sellman *et al.*, 2017) based closures of FSD for turbulent premixed combustion. However, most of these analyses (Boger *et al*., 1998; Cant and Bray, 1998; Charlette *et al*., 2002; Keppeler *et al*., 2014; Klein *et al*., 2016; Chakraborty and Klein., 2008a; Ma *et al*., 2013; Cant *et al.*, 1990; Candel *et al.*, 1990; Duclos *et al.*, 1993; Hawkes and Cant 2001a; Chakraborty and Cant, 2007; Hun and Huh, 2008; Katragadda *et al.*, 2011; Chakraborty *et al.*, 2011; Hernandez-Perez *et al.*, 2011; Reddy and Abraham, 2012; Chakraborty and Cant, 2013; Ma *et al.*, 2014; Sellman *et al.*, 2017) have been carried out based on single-step Arrhenius type chemistry and the effects of detailed chemical mechanism on the statistical behaviour of FSD and its transport are yet to be analysed in detail.

With the advances in computing power, it turned out that the well-known modelling challenges arising from the differential diffusion of heat and mass may be addressed by solving individual scalar transport equations with detailed chemistry models in RANS (Colin *et al*., 2003) or even

in LES (Li and Kong 2008, Vermorel *et al.*, 2009). Moreover, Colin *et al.* (2003) and Vermorel *et al*. (2009) solved transport equations for several major species, whereas the mean/filtered reaction rate has been closed by transporting one single FSD which may not behave necessarily similarly for all species. Thus, it is necessary to analyse the differences in the FSD transport for various definitions of the reaction progress variable (RPV) in a multi-species system.

Since FSD models were originally based on simple chemistry and in the corrugated flamelet (CF) regime, it is important to assess (i) their validity with detailed chemistry and (ii) their validity beyond the CF regime. As for (i), one of the most crucial aspects is the representation of the flame structures using different definitions of the reaction progress variable (RPV) associated with different species variables, and the present study is one of the first attempts to address this issue in detail. As for (ii), while the original FSD formulation was developed in the CF regime, in principle the generalised FSD $\Sigma_{gen} = \overline{|\nabla c|}$ is a field variable (Boger *et al*., 1998) and thus should be applicable irrespective of the regime. This raises the fundamental question about the possibility of using the original model under non-flamelet conditions, such as in the broken reaction zones regime, prior to any modifications are proposed.

For a multi-species system, various definitions of the RPV, c, are possible depending on the choice of the scalar variable. The influences of the choice of c on the statistical behaviour of Σ_{gen} and its modelling are yet to be discussed in open literature. The present analysis addresses the aforementioned gaps in the existing literature by assessing the FSD based reaction rate closure and the well-established sub-models of the FSD transport in the context of RANS using a three-dimensional direct numerical simulation (DNS) database of H_2-air flames with an equivalence ratio of 0.7 (which ensures that the flames remain globally thermo-diffusively neutral, in that the flame speed is insensitive to stretch (Im and Chen, 2002)). The simulation

parameters for this DNS database have been chosen such that the cases considered here represent typical combustion situations within the corrugated flamelets (CF), thin reaction zones (TRZ) and broken reaction zones (BRZ) regimes of premixed turbulent combustion. The main objectives of the present analysis are:

(1) to analyse the statistical behaviour of the FSD transport in different regimes of premixed turbulent combustion,

(2) to assess the performances of well-established existing closures for the FSD transport for different definitions of c.

The mathematical background and numerical implementation pertaining to this analysis are detailed in the next section. The results will be presented in the following section and subsequently discussed. The main findings are summarised and conclusions are drawn in the final section of this paper.

2. MATHEMATICAL BACKGROUND & NUMERICAL IMPLEMENTATION

The RPV is defined as: $c = (Y_0 - Y)/(Y_0 - Y_\infty)$, where Y is the mass fraction of a chosen species, and subscripts 0 and ∞ indicate the values in the unburned and fully burned gases, respectively. The RPV can alternatively be defined based on temperature as $c = (T - T_0)/(T_{ad} - T_0)$ where T, T_0 and T_{ad} are the instantaneous, unburned gas and adiabatic flame temperatures respectively. All definitions of c are identical if the Lewis number is unity for all species in the case of a single-step chemical mechanism; however, they differ in real flames due to the differential diffusion effects. In this analysis, RPVs based on temperature, H_2, O_2 and H_2O mass fractions are considered for H_2-air flames with an equivalence ratio of 0.7. This selection is not based on the fact that these species would represent the best definition of RPV for hydrogen or hydrocarbon flames. However, all of these species can be used to

define valid RPVs and they represent a bandwidth of Lewis numbers ranging from considerably smaller (H_2) to considerably larger than unity (O_2). The transport equation of $\tilde{c}$ is given by:

$$\partial(\bar{\rho}\tilde{c})/\partial t + \partial(\bar{\rho}\tilde{u}_j\tilde{c})/\partial x_j = \overline{\dot{w} + \partial[\rho D(\partial c/\partial x_j)]/\partial x_j} - \partial(\overline{\rho u_j'' c''})/\partial x_j \quad (1)$$

where ρ is the gas density, u_j is the j[th] component of velocity, $\tilde{q} = \overline{\rho q}/\bar{\rho}$ and $q'' = q - \tilde{q}$ are the Favre average and fluctuation of a general variable q, respectively. Here, $\dot{w} = -\dot{w}_Y/(Y_0 - Y_\infty)$ ($\dot{w} = \dot{w}_T/C_P(T_{ad} - T_0)$) for mass fraction (temperature) based RPV with $\dot{w}_Y$ ($\dot{w}_T$) being the net reaction rate of the corresponding species (the heat release rate), and C_P is the specific heat at constant pressure.

The terms on the right hand side of eq. 1 are unclosed. The first two terms on the RHS can be modelled as (Boger *et al.*, 1998): $\overline{\dot{w} + \nabla.(\rho D\nabla c)} = \overline{(\rho S_d)}_s\Sigma_{gen}$ where $\overline{(q)}_s = \overline{q|\nabla c|}/\Sigma_{gen}$ is the surface-averaged value of a general quantity q and $S_d = |\nabla c|^{-1}(Dc/Dt) = [\dot{w} + \nabla.(\rho D\nabla c)]/\rho|\nabla c|$ is the displacement speed. In the context of RANS, $\bar{\dot{w}} \gg \overline{\partial[\rho D(\partial c/\partial x_j)]/\partial x_j}$ (Chakraborty *et al.*, 2011) and thus $\bar{\dot{w}}$ can be closed if Σ_{gen} and $\overline{(\rho S_d)}_s$ are appropriately evaluated. In order to solve eq. 1, the turbulent scalar flux components ($\overline{\rho u_j'' c''}$) need to be modelled but this aspect is mostly independent of the FSD transport and its closure, and thus the discussion in this paper does not explicitly deal with the modelling of turbulent flux components. The closures of $\overline{\rho u_j'' c''}$ have been discussed elsewhere in detail (Veynante *et al.*, 1997; Chakraborty and Cant, 2009a,b) and thus will not be discussed in this paper. The closures of sub-grid scalar flux and Reynolds scalar flux for the database considered here can be found in Klein *et al.* (2018) and Papapostolou *et al.* (2018), respectively, and thus are not repeated here.

The transport equation for Σ_{gen} takes the following form (Cant *et al.*, 1990; Candel *et al.*, 1990; Duclos *et al.*, 1993; Veynante *et al.*, 1996; Hawkes and Cant 2001a; Chakraborty and Cant, 2007; Hun and Huh, 2008; Katragadda *et al.*, 2011; Chakraborty *et al.*, 2011; Hernandez-Perez *et al.*, 2011; Reddy and Abraham, 2012; Chakraborty and Cant, 2013; Ma *et al.*, 2014; Sellman *et al.*, 2017):

$$\partial\Sigma_{gen}/\partial t + \partial\left(\tilde{u}_j\Sigma_{gen}\right)/\partial x_j = \underbrace{-\partial\{\left[\overline{(u_k)_s} - \tilde{u}_k\right]\Sigma_{gen}\}/\partial x_k}_{T_1-turbulent\ transport} + \tag{2}$$

$$\underbrace{\overline{\left(\left(\delta_{\iota J} - N_\iota N_J\right)\partial u_\iota/\partial x_J\right)_s}\,\Sigma_{gen}}_{T_2-strain\ rate} \underbrace{-\partial\left[\overline{(S_d N_k)_s}\Sigma_{gen}\right]/\partial x_k}_{T_3-propagation} + \underbrace{\overline{(S_d\,\partial N_\iota/\partial x_\iota)_s}\Sigma_{gen}}_{T_4-curvature}$$

where $N = -\nabla c/|\nabla c|$ is the local flame normal vector. The distributions of ∇c and S_d are different for each scalar used for the RPV definition, and this is considered while evaluating all the terms of eq. 2.

A three-dimensional DNS (Arias *et al.*, 2016; Wacks *et al.*, 2016) database of H_2-air flames with an equivalence ratio of 0.7, employing a detailed chemical mechanism (Burke *et al.*, 2012) with 9 species and 19 chemical reactions, is considered here. The unburned gas temperature T_0 is taken to be 300K, which leads to an unstrained laminar burning velocity $S_L = 135.6$ cm/s and heat release parameter $\tau = (T_{ad} - T_0)/T_0 = 5.71$ (where T_{ad} is the adiabatic flame temperature) under atmospheric pressure. The numerical implementation pertaining to this database has been discussed elsewhere (Arias *et al.*, 2016; Wacks *et al.*, 2016) in detail and thus will not be repeated here. Turbulent inflow and outflow boundaries are taken in the direction of mean flame propagation and transverse boundaries are taken to be periodic. The inflow and outflow boundaries are specified using an improved version of the Navier Stokes characteristic boundary conditions (NSCBC) technique (Yoo *et al.*, 2005). The inflow turbulent velocity fluctuations are specified by scanning a plane through a frozen turbulent homogeneous

isotropic incompressible velocity fluctuation field, which was generated using a pseudo-spectral method (Rogallo, 1981) following the Passot-Pouquet spectrum (Passot and Pouquet, 1987). The temporal evolution of flame area has been monitored and the flame is considered to be statistically stationary when the flame area no longer varies with time. The inflow values of normalised root-mean-square turbulent velocity fluctuation u'/S_L , turbulent length scale to flame thickness ratio l_T/δ_{th}, Damköhler number $Da = l_T S_L/u'\delta_{th}$, Karlovitz number $Ka = (\rho_0 S_L \delta_{th}/\mu_0)^{0.5}(u'/S_L)^{1.5}(l_T/\delta_{th})^{-0.5}$ and turbulent Reynolds number $Re_t = \rho_0 u' l_T/\mu_0$ for all cases are presented in Table 1 where μ_0 is the unburned gas viscosity, $\delta_{th} = (T_{ad} - T_0)/\max|\nabla T|_L$ is the thermal flame thickness and the subscript 'L' is used to refer to unstrained laminar flame quantities. Cases A-C are representative of the CF ($Ka < 1$), TRZ ($1 < Ka < 100$) and BRZ ($Ka > 100$) regimes (Peters, 2000) of premixed combustion respectively.

The domain size is $20mm \times 10mm \times 10mm$ ($8mm \times 2mm \times 2mm$) in cases A and B (case C) and the domain has been discretised by a uniform Cartesian grid of $512 \times 256 \times 256$ ($1280 \times 320 \times 320$). Simulations have been carried out for $1.0t_e$, $6.8t_e$ and $6.7t_e$ (i.e. $t_e = l_T/u'$) for cases A-C respectively, and this simulation time remains comparable to several previous analyses (Boger *et al*., 1998; Charlette *et al*., 2002; Hun and Huh, 2008; Reddy and Abraham, 2012).

3. RESULTS & DISCUSSION

The distributions of RPV for the flames considered here are presented elsewhere (Arias *et al.*, 2016; Wacks *et al.*, 2016) and thus are not shown here. In statistically planar flames, $\tilde{c}$ is a unique function of the mean direction of flame propagation and thus all the terms are presented here as functions of $\tilde{c}$ for different definitions of RPV.

Statistical behaviour of the unclosed terms of the FSD transport equation

The variations of normalised values of $T_1 - T_4$ with $\tilde{c}$ for cases A-C are shown in Fig. 1 for different choices of RPV. Figure 1 shows that T_2 and T_4 predominantly act as the dominant source and sink terms respectively for all cases irrespective of the choice of RPV. However, T_4 assumes positive values for $\tilde{c} < 0.2$ in case A, whereas this term remains negative throughout the flame brush for cases B and C for all choices of RPV. The contributions of T_1 and T_3 assume both positive and negative values within the flame brush. The relative magnitudes of T_1 and T_3 in comparison to those of T_2 and T_4 remain small in the cases representing the TRZ and BRZ regimes (i.e. cases B and C), whereas the magnitudes of T_1, T_2 and T_3 remain comparable in the case representing the CF regime (i.e. case A). The above observation holds for all the different choices of RPV considered here. In cases B and C, the magnitudes of positive T_2 and negative T_4 remain comparable, whereas the magnitude of T_2 remains small in comparison to T_4 in case A for all definitions of RPV considered here. The dominant behaviour of T_2 and T_4 in all cases are consistent with scaling estimates presented earlier by Chakraborty and Cant (Chakraborty and Cant, 2013) in a simple chemistry DNS analysis. The implications of the choice of RPV on the modelling of $T_1 - T_4$ will be discussed next in this section.

Modelling of the turbulent transport term T_1

The modelling of T_1 depends on the closure of the turbulent flux of FSD $\left[\overline{(u_i)}_s - \widetilde{u_i}\right]\Sigma_{gen}$. A gradient transport (GT) hypothesis $\left[\overline{(u_k)}_s - \widetilde{u_k}\right]\Sigma_{gen} = -\left(\nu_t / S_{c_\Sigma}\right)\partial\Sigma_{gen}/\partial x_k$ (where $\nu_t = C_\mu \tilde{k}^2/\tilde{\varepsilon}$ is the eddy kinematic viscosity and S_{c_Σ} is the turbulent Schmidt number with $\tilde{k} = \overline{\rho u_i'' u_i''}/2\bar{\rho}$ and $\tilde{\varepsilon} = \overline{\mu\left(\partial u_i''/\partial x_j\right)\left(\partial u_i''/\partial x_j\right)}/\bar{\rho}$ being the turbulent kinetic energy and its dissipation rate, and $C_\mu = 0.09$ is a model parameter) is often employed for the closure of turbulent flux of FSD (Hawkes and Cant 2001a; Hernandez-Perez *et al.*, 2011; Ma *et al.*, 2014).

However, previous analyses (Chakraborty *et al.*, 2011; Chakraborty and Cant, 2013; Sellman *et al.*, 2017) suggested that the turbulent flux of FSD exhibits a counter-gradient behaviour when the turbulent flux of RPV $\overline{\rho u_1'' c''}$ shows a counter-gradient transport (CGT) and *vice versa*. Chakraborty and Cant (2011) modified an existing model (Veynante *et al.*, 1997) in order to make it capable of predicting both GT and CGT of FSD as:

$$\left[\overline{(u_\iota)}_s - \widetilde{u_\iota}\right]\Sigma_{gen} = (1-2\tilde{c})\overline{\rho u_\iota'' c''}\,\Sigma_{gen}/[\overline{\rho c''^2} + \bar{\rho}\tilde{c}(1-\tilde{c})] \quad (3)$$

The predictions of eq. 3 are shown alongside $\left[\overline{(u_\iota)}_s - \widetilde{u_\iota}\right]\Sigma_{gen}$ extracted from DNS data in Fig. 2 for cases A-C for all the different choices of RPV. Figure 2 indicates that the GT model does not adequately capture both the qualitative and quantitative behaviours of $\left[\overline{(u_\iota)}_s - \widetilde{u_\iota}\right]\Sigma_{gen}$ in cases A and B for all choices of RPV. Furthermore, in these cases the GT model predicts the wrong sign of $\left[\overline{(u_\iota)}_s - \widetilde{u_\iota}\right]\Sigma_{gen}$ in some locations of the flame brush, which is indicative of a CGT of Σ_{gen}. In contrast, eq. 3 is more successful in capturing the qualitative behaviour of $\left[\overline{(u_\iota)}_s - \widetilde{u_\iota}\right]\Sigma_{gen}$ despite having quantitative differences between the model prediction and DNS data for all cases irrespective of the choice of the RPV. A reasonable level of agreement between the predictions of the GT model and DNS data is obtained for case C for all choices of RPV and the performance of the GT model in this case remains comparable to that of the model given by eq. 3. The qualitative agreement between the GT model prediction and $\left[\overline{(u_\iota)}_s - \widetilde{u_\iota}\right]\Sigma_{gen}$ in case C suggests a GT of Σ_{gen} in this case. A CGT is obtained when flame normal acceleration dominates over turbulent fluctuations which can be quantified as $\tau S_L > u'$ (Veynante *et al.*, 1997) where $\tau = (T_{ad} - T_0)/T_0$ is the heat release parameter which is 5.71 for this database. Accordingly, cases A and B (where $\tau S_L > u'$) exhibit a CGT of Σ_{gen}, whereas a GT is obtained for case C (where $\tau S_L < u'$). The observations from Fig. 2 suggest that eq. 3 is capable of predicting predominantly CGT (GT) for cases A and B (case C).

Modelling of the tangential strain rate term T_2

The term T_2 is often modelled by splitting it into two components (Cant *et al.*, 1990; Candel *et al.*, 1990; Duclos *et al.*, 1993; Veynante *et al.*, 1996; Hawkes and Cant 2001a):

$$T_2 = \underbrace{\left[\delta_{ik} - \overline{(N_\iota N_k)}_s\right](\partial\widetilde{u}_\iota/\partial x_k)\Sigma_{gen}}_{T_{21}} + \underbrace{\overline{([\delta_{\iota k} - N_\iota N_k]\,\partial u_\iota''/\partial x_k)}_s\Sigma_{gen}}_{T_{22}} \quad (4)$$

Cant *et al.* (1990) proposed $\overline{(N_\iota N_k)}_s = \overline{(N_\iota)}_s\,\overline{(N_k)}_s + (\delta_{ik}/3)[1 - \overline{(N_l)}_s\,\overline{(N_l)}_s]$ (Cant-Pope-Bray (CPB) model) where $\overline{(N_k)}_s = -(\partial\bar{c}/\partial x_k)/\Sigma_{gen}$. Chakraborty and Cant (2011) suggested $\bar{c} = (1 + \tau g^{1.5}Le^{-0.26})\tilde{c}/[1 + \tau g^{1.5}Le^{-0.26}\tilde{c}]$ (where $g = \overline{\rho c''^2}/\,\bar{\rho}\tilde{c}(1-\tilde{c})$ is the segregation factor, Le is the Lewis number of the RPV), which is valid for both $Da < 1$ and $Da > 1$ flamelet combustion, and this expression can be used to evaluate $\overline{(N_k)}_s = -(\partial\bar{c}/\partial x_k)/\Sigma_{gen}$ for all cases for all definitions of RPV (not shown here).

An alternative model for $\overline{(N_\iota N_k)}_s$ was proposed by Veynante *et al.* (1996): $\overline{(N_\iota N_{k=\iota})}_s = \sum_{l\neq i}\widetilde{u_l''u_l''}/4\tilde{k}$ and $\overline{(N_\iota N_{k\neq\iota})}_s = \widetilde{u_\iota''u_k''}/2\tilde{k}$ (VPDM Model). Figure 3 reveals that the CPB model consistently captures the qualitative behaviour of T_{21} for all choices of RPV, but this model underestimates the magnitude of T_{21}. The VPDM model is more successful in terms of capturing the magnitude of T_{21} for all three cases despite a slight overprediction in case B. Experimental (Veynante *et al.*, 1996) and DNS (Chakraborty and Cant, 2006) results suggested that the unresolved part of $\overline{(N_\iota N_k)}_s$ does not remain isotropic, as assumed in the CPB model, whereas the VPDM model accounts for the anisotropy of $\overline{(N_\iota N_k)}_s - \overline{(N_\iota)}_s\overline{(N_k)}_s$. This difference is reflected in the superior performance of the VPDM model in Fig. 3. A similar observation was made by Chakraborty and Cant (2006) in the context of LES modelling using simple chemistry DNS data.

The two most popular models for T_{22} are the ones proposed by Cant *et al*. (1990) (i.e. $T_{22} = 0.28\sqrt{\tilde{\varepsilon}/\nu_0}\Sigma_{gen}$ henceforth referred to as the CPB model) and by Candel *et al*. (1990) (i.e. $T_{22} = a_0\Gamma_k\left(\tilde{\varepsilon}/\tilde{k}\right)\Sigma_{gen}$ henceforth referred to as the coherent flamelet model (CFM) model (Duclos *et al.*, 1993) where ν_0 is the kinematic viscosity in the unburned gas and is defined as $\nu_0 = \mu_0/\rho_0$ with μ_0 and ρ_0 being the unburned gas viscosity and density respectively, a_0 is a model constant (taken as $a_0 = 2.0$ following (Chakraborty *et al.*, 2011; Chakraborty and Cant, 2013)), and Γ_k is the efficiency function (Meneveau and Poinsot, 1991), which depends on $l_t S_L/\alpha_{T0}$ and $\sqrt{2\tilde{k}/3}\,/S_L$ with α_{T0} being the thermal diffusivity in the unburned gas, and $l_t = C_k\tilde{k}^{3/2}/\tilde{\varepsilon}$ is the local integral length scale, where C_k depends on the local Taylor micro-scale Reynolds number (Lindstedt and Vaos, 1999).

The predictions of the CPB and CFM models are compared to T_{22} extracted from the DNS data in Fig. 4 for cases A-C for different choices of RPV. Figure 4 shows that both CPB and CFM models significantly overpredict T_{22} for cases A and B. Moreover, the term T_{22} remains negative in the middle of the flame brush in case A, whereas T_{22} assumes negative values towards the burned gas side of the flame brush before vanishing altogether in case B. In contrast, both CPB and CFM models predict only positive values throughout the flame brush. In case C, the term T_{22} exhibits positive values throughout the flame brush and the qualitative agreement between the DNS data and the model predictions are improved, with the CFM model performing better quantitatively than CPB which overpredicts T_{22} throughout the flame brush.

The term T_{22} can be expressed as: $T_{22} = \overline{(e_\alpha \sin^2\alpha + e_\beta \sin^2\beta + e_\gamma \sin^2\gamma)|\nabla c|}$ where e_α, e_β and e_γ are the most extensive, intermediate and the most compressive eigenvalues of $e_{ij} = 0.5(\partial u_i''/\partial x_j + \partial u_j''/\partial x_i)$ and α, β and γ are the angles between ∇c and the eigenvectors

associated with e_α, e_β and e_γ respectively. It has been demonstrated elsewhere (Chakraborty and Swaminathan, 2007) that ∇c preferentially aligns collinearly with the eigenvector associated with e_α (i.e. high probability of $\sin^2\alpha \approx 0$) for $Da \gg 1$ flames (e.g. case A) where the strain rate due to flame normal acceleration overcomes turbulent straining. Thus, $T_{22} = \overline{(e_\alpha \sin^2\alpha + e_\beta \sin^2\beta + e_\gamma \sin^2\gamma)|\nabla c|}$ is likely to exhibit negative values in cases A and B. The effects of flame normal straining weaken with increasing Ka (Chakraborty and Swaminathan, 2007) (e.g. from case A to case B) and thus the likelihood of obtaining negative values of T_{22} is relatively smaller in case B than in case A. In contrast, ∇c preferentially aligns collinearly with the eigenvector associated with e_γ (i.e. high probability of $\sin^2\gamma \approx 0$) for $Da < 1$ combustion (e.g. case C) where turbulent straining overcomes the strain rate due to flame normal acceleration, and thus, T_{22} exhibits only positive values in case C.

Both CPB and CFM models neglect the effects of strain rate associated with flame normal acceleration (Katragadda *et al.,* 2011). The CPB model scales the strain rate in terms of the Kolmogorov time scale ($\sqrt{\nu_0/\tilde{\varepsilon}}$) which is strictly valid for passive material surfaces (Cant *et al.,* 1990). As flames resemble increasingly passive surfaces at higher Ka, the CPB model is poor in capturing the behaviour of T_{22} for cases A and B but improves for case C. As for the CFM model, which is based on the large-scale turbulent strain rate ($\tilde{\varepsilon}/\tilde{k} \sim u'/l_t$), the change of ∇c alignment with local principal strain rates induced by flame normal acceleration is not properly accounted for, although it may be argued that Γ_k can include such information. Moreover, both CPB and CFM models implicitly are based on the preferential collinear alignment between ∇c with the eigenvector associated with e_γ, which is valid only for case C.

It is worth noting that different efficiency factor Γ_k expressions have also been proposed in the context of LES (Charlette *et al*., 2002; Colin *et al.,* 2000) but applying them in the CFM model

does not improve its prediction significantly in cases A and B, and also does not capture the negative values of T_{22}. Chakraborty and Cant (Chakraborty *et al.,* 2011; Chakraborty and Cant, 2013) proposed a correction factor of the form $a_{corr} = a_{T22}(1-\tilde{c})^{\xi}/Le^{p}$ where a_{T22}, ξ and p are the model parameters for both CPB and CFM models but this is not considered in this analysis because this correction factor is not capable of predicting negative values of T_{22}.

It is worth noting that both CPB and CFM models have been proposed and assessed for simple chemistry mechanisms and unity Lewis number (Cant *et al.,* 1990; Candel *et al.,* 1990; Duclos *et al.,* 1993; Hawkes and Cant 2001a; Chakraborty and Cant, 2007; Hernandez-Perez *et al.,* 2011; Reddy and Abraham, 2012; Chakraborty and Cant, 2013; Ma *et al.,* 2014). Moreover, the assumptions behind the CPB and CFM models are also not consistent with the flame physics in cases A-C. For example, the surface-averaged tangential strain rate for the CPB model is taken to scale with the Kolmogorov time scale $\tau_{\eta} = \sqrt{\nu_0/\tilde{\varepsilon}}$, which is valid for material surfaces (Yeung *et al*., 1990) but not valid for a flame which propagates normal to itself (Cant *et al*., 1990). By contrast, the CFM model scales with the surface-averaged tangential strain rate with large-scale turbulent straining $\tilde{k}/\tilde{\varepsilon}$ but the efficiency function Γ_k allows for different extents of flame wrinkling (Meneveau and Poinsot, 1991). However, Γ_k is calibrated based on two-dimensional unsteady flame-vortex interaction, which is not representative of actual flame-turbulence interaction. Both CPB and CFM models do not explicitly account for chemical time-scale and ∇c alignment with local principal strain rates. Although most previous assessments of the CPB and CFM models have been carried out for simple single-step chemistry, the analysis by Chakraborty and Cant (2011, 2013), Katragadda *et al*. (2011) and Sellmann *et al*. (2017) also reported unsatisfactory predictions of the CPB and CFM models. Katragadda *et al*. (2011) and Sellmann *et al*. (2017) recently modelled $T_D = \overline{(\partial u_i''/\partial x_i)}_s \Sigma_{gen}$ and $(-T_N) = -\overline{\left(N_i N_j \partial u_i''/\partial x_j\right)}_s \Sigma_{gen}$ separately, and explicitly accounted for the alignment

statistics of ∇c with local principal strain rates, but this approach is not yet established and is beyond the scope of current work.

Modelling of the combined propagation and curvature terms ($T_3 + T_4$)

The combined contribution of $(T_3 + T_4)$ is usually modelled together in the following manner due to their displacement speed S_d dependence (Hun and Huh, 2008; Chakraborty *et al.*, 2011; Chakraborty and Cant, 2013; Sellman *et al.*, 2017):

$$(T_3 + T_4) = -\frac{\partial}{\partial x_i}\left[\frac{\rho_0 S_L}{\bar{\rho}}\overline{(N_i)}_s\Sigma_{gen}\right] + \frac{\rho_0 S_L}{\bar{\rho}}\frac{\partial\overline{(N_i)}_s}{\partial x_i}\Sigma_{gen} - \beta_0\alpha_N\frac{(\bar{c}-c_{cp})S_L\Sigma_{gen}^2}{\bar{c}(1-\bar{c})} \qquad (5)$$

where $\alpha_N = 1 - \overline{(N_k)}_s\,\overline{(N_k)}_s$ and β_0 and c_{cp} are the model parameters (Chakraborty *et al.*, 2011; Chakraborty and Cant, 2013; Sellman *et al.*, 2017). The model parameter β_0 has to satisfy $\beta_0 > 1$ in order to ensure realisability (i.e. $\Sigma_{gen} \geq 0$) (Duclos *et al.*, 1993; Hawkes and Cant, 2001b), and this has been confirmed in previous simple chemistry DNS studies (Chakraborty *et al.*, 2011; Chakraborty and Cant, 2013; Sellman *et al.*, 2017), which suggested $\beta_0 = 8.0$ and $c_{cp} = 0.55[1 - \exp(-Le^{-2.5})]$. It has been found for this database that the optimum values of these model parameters depend on the definition of RPV and they also change from one case to another. The optimum values of β_0 and c_{cp} for cases A-C are listed in Table 2.

Figure 5 shows that eq. 5 accurately predicts $(T_3 + T_4)$ for β_0 and c_{cp} values listed in Table 2 in cases A-C. Previous analyses (Chakraborty *et al.*, 2011; Chakraborty and Cant, 2013) indicated that β_0 and c_{cp} depend on Le and may also have some Re_t dependence. This explains the different model parameters for different cases and for the choices of H_2, O_2 and H_2O, which have different diffusivities. It has also been shown (Chakraborty and Cant, 2005; Chakraborty *et al.*, 2008; Chakraborty and Klein, 2008b) that the stretch rate dependence of S_d

significantly affects the statistical behaviours of the curvature and propagation terms, and Le influences these statistics as well. Although a single-step chemical mechanism captures the generic qualitative nature of the stretch rate dependence of S_d, these statistics are quantitatively different for different choices of RPV in H_2-air flames (not shown here). Moreover, in H_2-air flames $\dot{w}$ assumes its peak value at a much smaller value of c for temperature-based RPV (for which Le of the RPV is exactly equal to unity) than the value of c at which $\dot{w}$ assumes its peak value for H_2, O_2 and H_2O mass fraction-based RPVs (and also for single step irreversible Arrhenius type chemistry which is not shown here). Thus, the optimum values of β_0 and c_{cp} show dependence on the choice of RPV, and these values are different from those reported previously (Hun and Huh, 2008; Chakraborty *et al.*, 2011; Chakraborty and Cant, 2013) based on simple chemistry DNS analyses.

A comparison between the magnitudes of T_3 and T_4 in Fig. 1 reveals that the magnitude of T_4 is much greater than T_3 and thus eq. 5 principally models the unresolved part of the curvature term T_4. The curvature term T_4 can be split in terms of displacement speed components as (Chakraborty and Cant, 2007): $T_4 = 2\overline{[(S_r + S_n)\kappa_m]}_s\Sigma_{gen} - 4\overline{(D\kappa_m^2)}_s\Sigma_{gen}$ where $S_r = \dot{w}/\rho|\nabla c|$ and $S_n = \vec{N}.\nabla(\rho D\vec{N}.\nabla c)/\rho|\nabla c|$ are the reaction and normal diffusion components of displacement speed. According to Peters (2000), the contribution of $-4\overline{(D\kappa_m^2)}_s\Sigma_{gen}$ strengthens with increasing Ka. The magnitudes of the first two terms on the right hand side of eq. 5 remain small in comparison to $(-\beta_0\alpha_N\left(\bar{c} - c_{cp}\right)S_L\Sigma_{gen}^2/\bar{c}(1 - \bar{c}))$ and this term is principally responsible for sink contribution of $(T_3 + T_4)$ (not shown here). Thus, the optimum value of β_0 shows an increasing trend from case A to case C in order to account for the strengthening contribution of $-4\overline{(D\kappa_m^2)}_s\Sigma_{gen}$ with increasing Ka.

The observed lack of universal model parameter β_0 behaviour is attributed to the lack of the involvement of displacement speed S_d and its curvature $\nabla.\vec{N}/2$ dependence in the in the model for $(T_3 + T_4) = -\nabla \cdot \left[\left(S_d\vec{N}\right)_s \Sigma_{gen}\right] + \overline{2\left(S_d\nabla.\vec{N}\right)_s \Sigma_{gen}}$ given by eq. 5. As the displacement speed statistics including its curvature dependence change with the definition of RPV and also with the regime of combustion, the optimum value of β_0 shown in Table 2 exhibits dependence on the RPV definition and combustion regime.

Mean reaction rate closure by $\boldsymbol{\Sigma_{gen}}$

Finally, the closure of the mean reaction rate $\bar{\dot{w}}$ is discussed. First, in the context of RANS the contribution of $\overline{\nabla \cdot (\rho D \nabla c)}$ in statistically planar flames remains small in comparison with the mean reaction rate $\bar{\dot{w}}$, and thus $\bar{\dot{w}}$ can be modelled as: $\bar{\dot{w}} \approx \overline{(\rho S_d)}_s \Sigma_{gen}$. The surface-averaged value of the density-weighted displacement speed $\overline{(\rho S_d)}_s$ is often approximated as $\overline{(\rho S_d)}_s \approx \rho_o S_L$ (Boger *et al.*, 1998; Hawkes and Cant 2001a; Hernandez-Perez *et al.*, 2011; Ma *et al.*, 2014).

The mean reaction rate $\bar{\dot{w}}$ obtained from DNS data is compared to $\rho_0 S_L \Sigma_{gen}$ in Fig. 6 for cases A-C for different choices of RPV. Figure 6 shows that $\rho_0 S_L \Sigma_{gen}$ captures the qualitative behaviour of $\bar{\dot{w}}$ for all cases for different choices of RPV. However, the extent of quantitative agreement depends on the case and also on the choice of RPV. In cases A and B, $\rho_0 S_L \Sigma_{gen}$ accurately predicts $\bar{\dot{w}}$ for the temperature based RPV, whereas $\rho_0 S_L \Sigma_{gen}$ slightly underpredicts (overpredicts) $\bar{\dot{w}}$ towards the unburned (burned) gas side of the flame brush for RPVs defined based on the mass fractions of H_2O and O_2. However, $\rho_0 S_L \Sigma_{gen}$ for the H_2 mass fraction based RPV underestimates $\bar{\dot{w}}$, and the disagreement between $\rho_0 S_L \Sigma_{gen}$ and $\bar{\dot{w}}$ is the strongest for the H_2 based RPV out of all choices of RPVs. Note that Le for H_2 is

significantly smaller than unity and previous analysis based on simple chemistry DNS (Chakraborty *et al.*, 2011; Sellman *et al.*, 2017) revealed that $\rho_0 S_L \Sigma_{gen}$ significantly underpredicts $\overline{\dot{w}}$ for RPVs with $Le \ll 1$. In case C, $\rho_0 S_L \Sigma_{gen}$ slightly overpredicts (underpredicts) $\overline{\dot{w}}$ towards the unburned (burned) gas side of the flame brush for all choices of RPV. This underprediction is most prominent in the case of the H_2 mass fraction based RPV.

Figure 6 also shows that the quantitive prediction by $\rho_0 S_L \Sigma_{gen}$ becomes less accurate for case C. The effects of flame stretching strengthen with increasing Ka and $\overline{(\rho S_d)}_s$ cannot be approximated by $\rho_o S_L$ for the flames in the BRZ regime (e.g. case C). Recent studies (Klein *et al*., 2016; Chakraborty and Cant, 2007; Sabelnikov *et al.*, 2017) showed that the approximation $\overline{(\rho S_d)}_s \approx \rho_o S_L$ leads to incorrect behaviour even for the CF and TRZ regimes of combustion, and thus improved modelling of $\overline{(\rho S_d)}_s$ is needed to extend the FSD-based closures for high Karlovitz number combustion and to ensure the fidelity of the prediction of $\overline{\dot{w}}$. Furthermore, Fig. 6 indicates that the transport equation of a single FSD might not be sufficient for $\overline{\dot{w}}$ closures of all the major species for a multi-species system.

Final comments on model performances for different regimes

The optimal combinations of the closure models for the unclosed terms of the FSD transport equation for different combustion regimes for different definitions of RPVs are summarised in Table 3. It can be seen from Table 3 that the model performances for the unclosed terms of the FSD transport equation are comparable for different definitions of RPVs for terms T_1, T_{21}, T_{22} but the optimal model for T_{22} in case C is different to cases A and B. Moreover, the model performances for $(T_3 + T_4)$ and $\overline{\dot{w}}$ depend on the choice of RPV and shows the strongest deviations for H_2 based RPV. It is worth noting that $|\nabla c|$ distributions for cases A-C are mostly similar for O_2 and H_2O based RPVs, whereas smaller values of $|\nabla c|$ are more likely in

case C than in cases A and B (Chakraborty *et al*., 2018). This behaviour has been explained based on the differences in strain rate and displacement speed statistics for different species by Chakraborty *et al*. (2018). Case C nominally represents the broken reaction zones regime where energetic turbulent eddies penetrate into the flame structure and also in the reaction zone. This effect is particularly important for the H_2 mass fraction based RPV because the reaction zone thickness is relatively thicker than O_2 and H_2O based RPVs due to smaller Lewis number of H_2 than O_2 and H_2O (e.g. $Le_{H_2} \ll 1$, and Le_{O_2} and Le_{H_2O} are close to unity). Most existing FSD based models have been proposed for simple chemistry mechanisms and unity Lewis number conditions (Boger *et al*., 1998; Cant and Bray, 1998; Charlette *et al*., 2002; Keppeler *et al*., 2014; Klein *et al*., 2016; Chakraborty and Klein., 2008a; Ma *et al*., 2013; Cant *et al*., 1990; Candel *et al.,* 1990; Duclos *et al.,* 1993; Hawkes and Cant 2001a; Chakraborty and Cant, 2007; Hernandez-Perez *et al.,* 2011; Reddy and Abraham, 2012; Chakraborty and Cant, 2013; Ma *et al.,* 2014). Thus, it is perhaps not surprising that the existing models in some cases do not show a good agreement with DNS data for the H_2 based RPV because $Le_{H_2} \ll 1$, whereas the model performances for O_2 and H_2O based RPVs remain comparable because the Lewis numbers of O_2 and H_2O are close to unity.

4. CONCLUSIONS

The implications of the choice of RPV on the performances of the well-established sub-models of the Σ_{gen} transport and the FSD based $\bar{\dot{w}}$ closure have been analysed in the context of RANS using a detailed chemistry DNS database of freely-propagating thermo-diffusively neutral H_2-air flames spanning the CF, TRZ and BRZ regimes of combustion. For this analysis, the RPV has been defined based on normalised H_2, O_2 and H_2O mass fractions and also using the non-dimensional temperature. It has been found that the performances of the closures for turbulent flux of FSD, and tangential strain rate term remain mostly unaffected by the choice

of RPV. However, both CPB and CFM models for the unresolved tangential strain rate term have been found not to perform well for the flames representing the CF and TRZ regimes of premixed combustion but the model performances are found to be relatively better for the flame belonging to the BRZ regime. The performance of a well-established existing model for the combined propagation and curvature terms has been found to be significantly dependent on the choice of RPV. Furthermore, the approximation given by $\overline{(\rho S_d)}_s \approx \rho_o S_L$ has also been found to be dependent on the choice of RPV and this approximation has been found to be especially unsatisfactory for all choices of RPV in the BRZ regime. Detailed explanations have been provided for the observed performances of the models for different combustion regimes and RPV definitions.

ACKNOWLEDGEMENTS

Part of the work presented in this study was sponsored by competitive research funding from King Abdullah University of Science and Technology (KAUST) and Engineering and Physical Sciences Research Council, UK The work made use of computational resources at KAUST Supercomputing Laboratory and ARCHER.

REFERENCES

Arias, P.G., Chaudhuri, S., Uranakara, H.A., Im, H.G. 2016. Direct numerical simulations of statistically stationary turbulent premixed flame, Combust. Sci. Technol., 188, 1182.

Boger, M., Veynante, D., Boughanem, H., Trouvé, A. 1998. Direct Numerical Simulation analysis of flame surface density concept for Large Eddy Simulation of turbulent premixed combustion, Proc. Combust. Inst., 27, 917.

Burke, M.P., Chaos, M., Ju, Y. Dryer, F.L., Klippenstein, S.J. 2012. Comprehensive H2-O2 kinetic model for high-pressure combustion, Int. J. Chem. Kin., 44, 444.

Candel, S.M., Poinsot, T.J. 1990. Flame stretch and the balance equation for the flame area, Combust. Sci. Technol., 70, 1- 15.

Candel, S., Veynante, D., Lacas, F., Maistret, E., Darabhia, N., Poinsot, T. 1990. Coherent Flamelet Model: Applications and recent extensions, in: B.E. Larrouturou (Ed.), Recent Advances in Combustion Modelling, World Scientific, Singapore, 19.

Cant, R.S., Bray, K.N.C. 1988. Strained laminar flamelet calculations of premixed turbulent combustion in a closed vessel, Proc. Combust. Inst., 22, 791.

Cant, R.S., Pope, S.B., Bray, K.N.C. 1990. Modelling of flamelet surface to volume ratio in turbulent premixed combustion, Proc. Combust. Inst., 27, 809.

Chakraborty, N., Cant, R.S. 2005. Effects of strain rate and curvature on Surface Density Function transport in turbulent premixed flames in the thin reaction zones regime, Phys. Fluids, 17, 65108.

Chakraborty, N., Cant, R.S. 2006. Statistical behaviour and modelling of flame normal vector in turbulent premixed flames, Numer. Heat Trans. A, 50, 623.

Chakraborty, N., Cant, R. S. 2007. A priori analysis of the curvature and propagation terms of the flame surface density transport equation for large eddy simulation, Phys. Fluids, 19, 105101.

Chakraborty, N., Cant, R.S. 2009a Physical insight and modelling for Lewis number effects on turbulent heat and mass transport in turbulent premixed flames, Numer. Heat Trans. A, 55,8,762.

Chakraborty, N., Cant, R.S. 2009b Effects of Lewis number on turbulent scalar transport and its modelling in turbulent premixed flames, Combust. Flame, 156, 1427.

Chakraborty, N., Cant, R.S. 2011. Effects of Lewis number on Flame Surface Density transport in turbulent premixed combustion, Combust. Flame, 158, 1768.

Chakraborty, N., Cant, R.S. 2013. Turbulent Reynolds number dependence of Flame Surface Density transport in the context of Reynolds Averaged Navier Stokes Simulations, Proc. Combust. Inst., 34, 1347.

Chakraborty, N., Swaminathan, N. 2007. Influence of Damköhler number on turbulence-scalar interaction in premixed flames, Part I: Physical Insight, Phys. Fluids, 19, 045103.

Chakraborty, N., Klein, M. 2008a. A-priori direct numerical simulation assessment of algebraic flame surface density models for turbulent premixed flames in the context of large eddy simulation, Phys. Fluids, 20, 085108.

Chakraborty, N., Klein, M. 2008b. Influence of Lewis number on the Surface Density Function transport in the thin reaction zones regime for turbulent premixed flames, Phys. Fluids, 20, 065102.

Chakraborty, N., Hawkes, E.R., Chen, J.H., Cant, R.S. 2008. Effects of strain rate and curvature on Surface Density Function transport in turbulent premixed CH_4-air and H_2-air flames: A comparative study, Combust. Flame, 154, 259.

Chakraborty, N., Klein, M., Alwazzan, D., Im, H. G. 2018. Surface Density Function statistics in Hydrogen-air flames for different turbulent premixed combustion regimes, Combust. Sci. Technol., doi.org/10.1080/00102202.2018.1480015.

Charlette, F., Meneveau, C., Veynante, D. 2002 A power law wrinkling model for LES of premixed turbulent combustion, Part I: Non dynamic formulation and initial tests, Combust. Flame, 131, 159.

Colin, O., Ducros, F., Veynante, D., Poinsot, T. 2000. A thickened flame model for large eddy simulations of turbulent premixed combustion, Phys. Fluids A , 12, 1843.

Colin, O, Benkenida A. and Angelberger, C., 2003. 3D Modeling of Mixing, Ignition and Combustion, Phenomena in Highly Stratified Gasoline Engines, Oil & Gas Science and Technology – Rev. IFP, 58:1, 47-62.

Duclos, J.M., Veynante, D., Poinsot, T. 1993. A comparison of flamelet models for turbulent premixed combustion, Combust. Flame, 95, 101.

Hernandez-Perez, F.E., Yuen, F. T. C., Groth, C.P.T., Gülder, Ö. L. 2011. LES of a laboratory-scale turbulent premixed Bunsen flame using FSD, PCM-FPI and thickened flame models, Proc. Combust. Inst., 33, 1365.

Hawkes, E.R., Cant, R.S. 2001a. Implications of a flame surface density approach to large eddy simulation of premixed turbulent combustion, Combust. Flame, 126, 1617.

Hawkes, E.R., Cant, R.S. 2001b. Physical and numerical realizability requirements for flame surface density approaches to large-Eddy and reynolds averaged simulation of premixed turbulent combustion, Combust. Theory Model., 5, 699.

Hun, I., Huh, K.Y. 2008. Roles of displacement speed on evolution of flame surface density for different turbulent intensities and Lewis numbers in turbulent premixed combustion, Combust. Flame, 152, 194.

Im, H.G., Chen, J.H. 2002. Preferential diffusion effects on the burning rate of interacting turbulent premixed Hydrogen-Air flames, Combust. Flame, 126, 246.

Katragadda, M., Malkeson, S.P., Chakraborty, N. 2011. Modelling of the tangential strain rate term of the Flame Surface Density transport equation in the context of Reynolds Averaged Navier Stokes Simulation, Proc. Combust. Inst., 33, 1429.

Keppeler, R., Tangermann, E., Allaudin, U., Pfitzner, M. 2014. LES of Low to High Turbulent Combustion in an Elevated Pressure Environment, Flow Turb. Combust., 92, 767.

Klein, M., Chakraborty, N., Pfitzner, M. 2016. Analysis of the combined modelling of subgrid transport and filtered flame propagation for premixed turbulent combustion, Flow Turb. Combust., 96, 921.

Klein, M., Kasten, C., Chakraborty, N., Im, H.G. 2018 Turbulent scalar fluxes in Hydrogen-Air premixed flames at low and high Karlovitz numbers, Combust. Theor. Modell., doi.org/10.1080/13647830.2018.1468034.

Knikker, R., Veynante, D., Meneveau, C. 2002. A priori testing of a similarity model for large eddy simulations of turbulent premixed combustion, Proc. Combust. Inst., 29, 2105.

Li S.C. and Kong Y.H., 2008. Diesel combustion modelling using LES turbulence model with detailed chemistry, Combust. Theory Model. 12:205–219.

Lindstedt, R.P., Vaos, E.M. 1999. Modelling of premixed turbulent flames with second moment methods, Combust. Flame, 116, 461.

Ma, T., Stein, T.O., Chakraborty, N., Kempf, A.M. 2013. A posteriori testing of algebraic flame surface density models for LES, Combust. Theor. Modell., 17, 431.

Ma, T., Stein, T.O., Chakraborty, N., Kempf, A.M. 2014. A-posteriori testing of the Flame Surface Density transport equation for LES, Combust. Theory Modell., 18, 32.

Meneveau, C., Poinsot, T. 1991. Stretching and quenching of flamelets in premixed turbulent combustion, Combust. Flame, 86, 311.

Papapostolou, V., Chakraborty, N., Klein, M., Im, H. G. 2018.Statistics of scalar flux transport of major species in different premixed turbulent combustion regimes for turbulent H2-air flames, Proc. Turb. Heat and Mass Trans. 2018, 10th -13th July, Rio de Jeneiro, Brazil, 2018.

Passot, T., Pouquet, A. 1987. Compressible Turbulence with a perfect gas law: A numerical. approach, J. Fluid Mech., 181, 441.

Peters, N. 2000. Turbulent Combustion, Cambridge Monograph on Mechanics, Cambridge University Press, Cambridge.

Reddy, H., Abraham, J. 2012. Two-dimensional direct numerical simulation evaluation of the flame-surface density model for flames developing from an ignition kernel in lean methane/air mixtures under engine conditions, Phys. Fluids, 24,105108.

Rogallo, R.S. 1981. Numerical experiments in homogeneous turbulence, NASA Technical Memorandum 81315, NASA Ames Research Center, California.

Sabelnikov, V., Lipatnikov, A.N., Chakraborty, N., Nishiki, S., Hasagawa, T. 2017. A balance equation for the mean rate of product creation in premixed turbulent flames, Proc. Combust. Inst., 36, 1893.

Sellmann, J., Lai, J., Chakraborty, N., Kempf, A.M. 2017. Flame Surface Density based modelling of head-on quenching of turbulent premixed flames, Proc. Combust. Inst., 36, 1817.

Veynante, D., Piana, J., Duclos, J.M., Martel, C. 1996. Experimental analysis of flame surface density models for premixed turbulent combustion, Proc. Combust. Inst., 26, 413.

Veynante, D., Trouvé, A., Bray, K.N.C., Mantel, T. 1997. Gradient and counter-gradient scalar transport in turbulent premixed flames, Proc. Combust. Inst., 26, 413.

Vermorel O., Richard, S., Colin, O., Angelberger, C., Benkenida, A. and Veynante, D. 2009. Towards the understanding of cyclic variability in a spark ignited engine using multicycle LES, Combust. Flame 156:525–1541.

Wacks, D.H., Chakraborty, N., Klein, M., Arias, P.G., Im, H.G. 2016. Flow topologies in Podifferent regimes of premixed turbulent combustion: A direct numerical simulation analysis, Phys. Rev. F, 1, 083401.

Yoo, C.S., Wang, Y., Trouve, A., Im, H.G. 2005. Characteristic boundary conditions for direct simulations of turbulent counterflow flames, Combust. Theor. Modell., 9, 617.

Yeung, P.K., Girimaji, S.S., Pope, S.B. 1990. Straining and scalar dissipation on material surfaces in turbulence: implications for flamelets, Combust. Flame, 79, 340.

TABLES

Case	u'/S_L	l_T/δ_{th}	Re_t	Da	Ka
A	0.7	14.0	227	20.0	0.75
B	5	14.0	1623	2.8	14.4
C	14	4.0	1298	0.29	126

Table 1: List of inflow turbulence parameters

	Model parameters	$c(\mathbf{H_2})$	$c(\mathbf{O_2})$	c **(**$\mathbf{H_2O}$**)**	c**(T)**
Case A	β_0	4.0	4.5	2.5	4.0
	c_{cp}	0.45	0.65	0.3	0.4
Case B	β_0	3.5	4.0	3.0	4.0
	c_{cp}	0.2	0.6	0.3	0.2
Case C	β_0	11.0	4.0	8.0	11.0
	c_{cp}	0.1	0.1	0.2	0.1

Table 2: Optimum values of β_0 and c_{cp} for different RPV definitions for cases A-C

	CF (Case A)				TRZ (Case B)				BRZ (Case C)			
	T	H_2	H_2O	O_2	T	H_2	H_2O	O_2	T	H_2	H_2O	O_2
$\boldsymbol{T_1}$	$\left[\overline{(u_i)}_s - \widetilde{u_i}\right]\Sigma_{gen} = (1-2\tilde{c})\overline{\rho u_i'' c''}\,\Sigma_{gen}/[\overline{\rho c''^2} + \bar{\rho}\tilde{c}(1-\tilde{c})]$ Performance is similar for different choices of RPV											
$\boldsymbol{T_{21}}$	$\overline{(N_i N_{k=i})}_s = \sum_{l\neq i}\widetilde{u_l'' u_l''}/4\tilde{k}$ and $\overline{(N_i N_{k\neq i})}_s = \widetilde{u_i'' u_k''}/2\tilde{k}$ Performance is similar for different choices of RPV											
$\boldsymbol{T_{22}}$	Neither CPB nor CFM model performs well. The prediction of the CPB model is closer to the DNS data in magnitude. The expression for the CPB model is given below: $T_{22} = 0.28\sqrt{\tilde{\varepsilon}/\nu_0}\Sigma_{gen}$ Performance is similar for different choices of RPV				$T_{22} = a_0\Gamma_k(\tilde{\varepsilon}/\tilde{k})\Sigma_{gen}$, a_0 = 2.0, Γ_k- efficiency function Performance is similar for different choices of RPV							
$\boldsymbol{T_3 + T_4}$	$(T_3+T_4) = -\frac{\partial}{\partial x_i}\left[\frac{\rho_0 S_L}{\bar{\rho}}\overline{(N_i)}_s\Sigma_{gen}\right] + \frac{\rho_0 S_L}{\bar{\rho}}\frac{\partial\overline{(N_i)}_s}{\partial x_i}\Sigma_{gen} - \beta_0\alpha_N\frac{(\bar{c}-c_{cp})S_L\Sigma_{gen}^2}{\bar{c}(1-\bar{c})}$ $\alpha_N = 1 - \overline{(N_k)}_s\,\overline{(N_k)}_s$, optimal, RPV dependent, β_0 and c_{cp} provided in Table 2											
$\bar{\dot{w}}$	$\bar{\dot{w}} = \rho_0 S_L \Sigma_{gen}$ Performance is the best for T based RPV and the deviation from DNS data is the highest for H_2 based RPV.											

Table 3: Summary of optimal combination of the closure models for the unclosed terms of the FSD transport equation for different combustion regimes for different definitions of RPVs.

FIGURE CAPTIONS

Fig. 1: Variations of $T_i \times \delta_{th}^2/S_L$ (where solid line, dashed line, dashed dotted line, and line with circles, are used for $i = 1-4$ respectively) with $\tilde{c}$ for cases A-C from left to right columns respectively. The results in Figs. 1-6 for RPV definitions based on temperature, H_2, H_2O and O_2 mass fractions are shown by black, red, green and blue lines respectively.

Fig. 2: Variation of $\left[\overline{(u_i)}_s - \tilde{u}_i\right]\Sigma_{\text{gen}} \times \delta_{th}/S_L$ (solid lines for DNS data) along with the predictions of the gradient hypothesis (dotted line) and eq. 3 (broken line) with $\tilde{c}$ for cases A-C from left to right columns respectively.

Fig. 3: Variation of $T_{21} \times \delta_{th}^2/S_L$ (solid lines for DNS data) along with the predictions of the CPB (broken line) and VPDM (dotted line) models with $\tilde{c}$ for cases A-C from left to right columns respectively.

Fig. 4: Variation of $T_{22} \times \delta_{th}^2/S_L$ (solid lines for DNS data) along with the predictions of the CPB (broken line) and CFM (dotted line) models with $\tilde{c}$ for cases A-C from left to right columns respectively.

Fig. 5: Variation of $(T_3 + T_4) \times \delta_{th}^2/S_L$ (solid lines for DNS data) along with the predictions of eq. 5 with β_0 given in Table 2 (broken line) with $\tilde{c}$ for cases A-C from left to right columns respectively.

Fig. 6: Variations of $\overline{\dot{w}} \times \delta_{th}/\rho_0 S_L$ (solid line), along with $\rho_0 S_L \Sigma_{gen} \times \delta_{th}/\rho_0 S_L$ (broken line) with $\tilde{c}$ for cases A-C from left to right columns respectively.

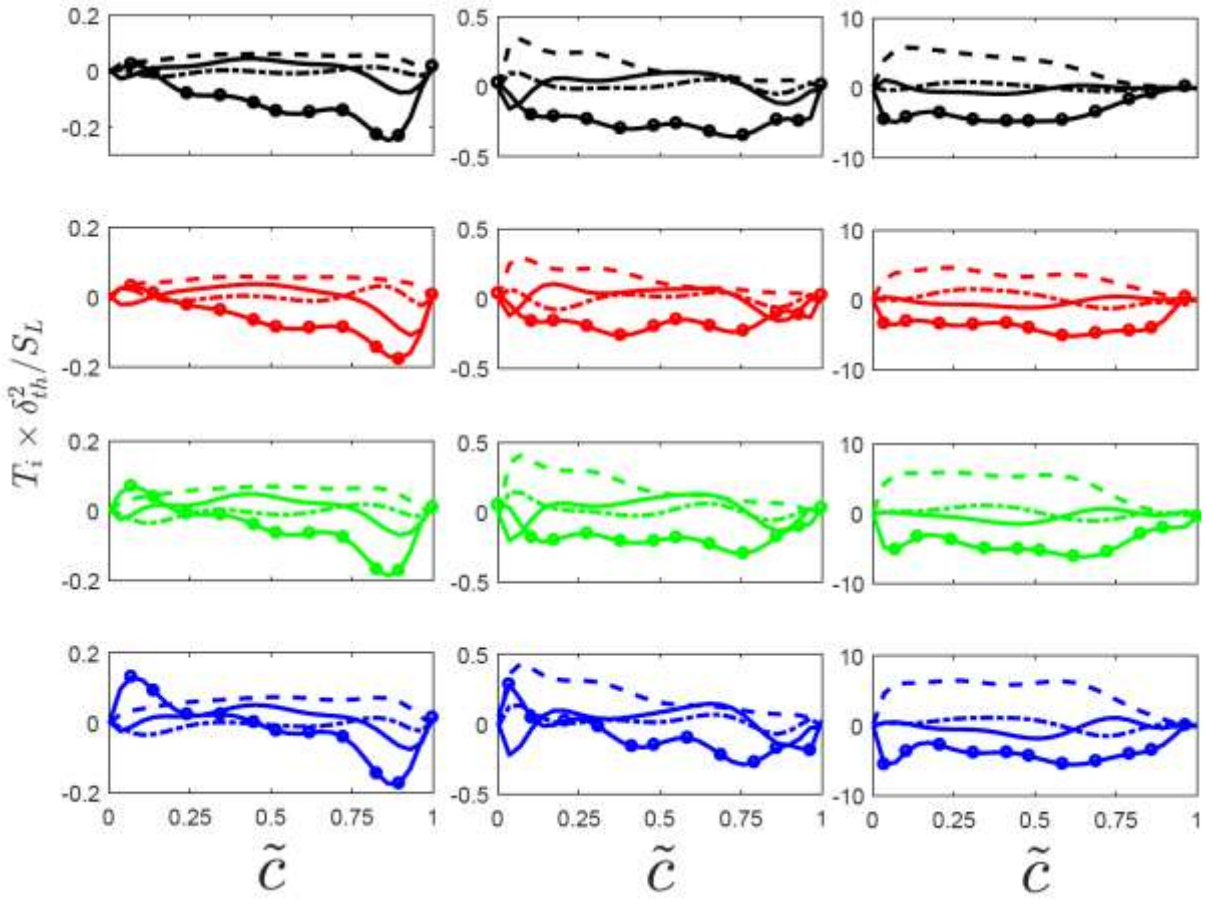

Fig. 1: Variations of $T_i \times \delta_{th}^2/S_L$ (where solid line, dashed line, dashed dotted line, and line with circles, are used for $i = 1 - 4$ respectively) with $\tilde{c}$ for cases A-C from left to right columns respectively. The results in Figs. 1-6 for RPV definitions based on temperature, H_2, H_2O and O_2 mass fractions are shown by black, red, green and blue lines respectively.

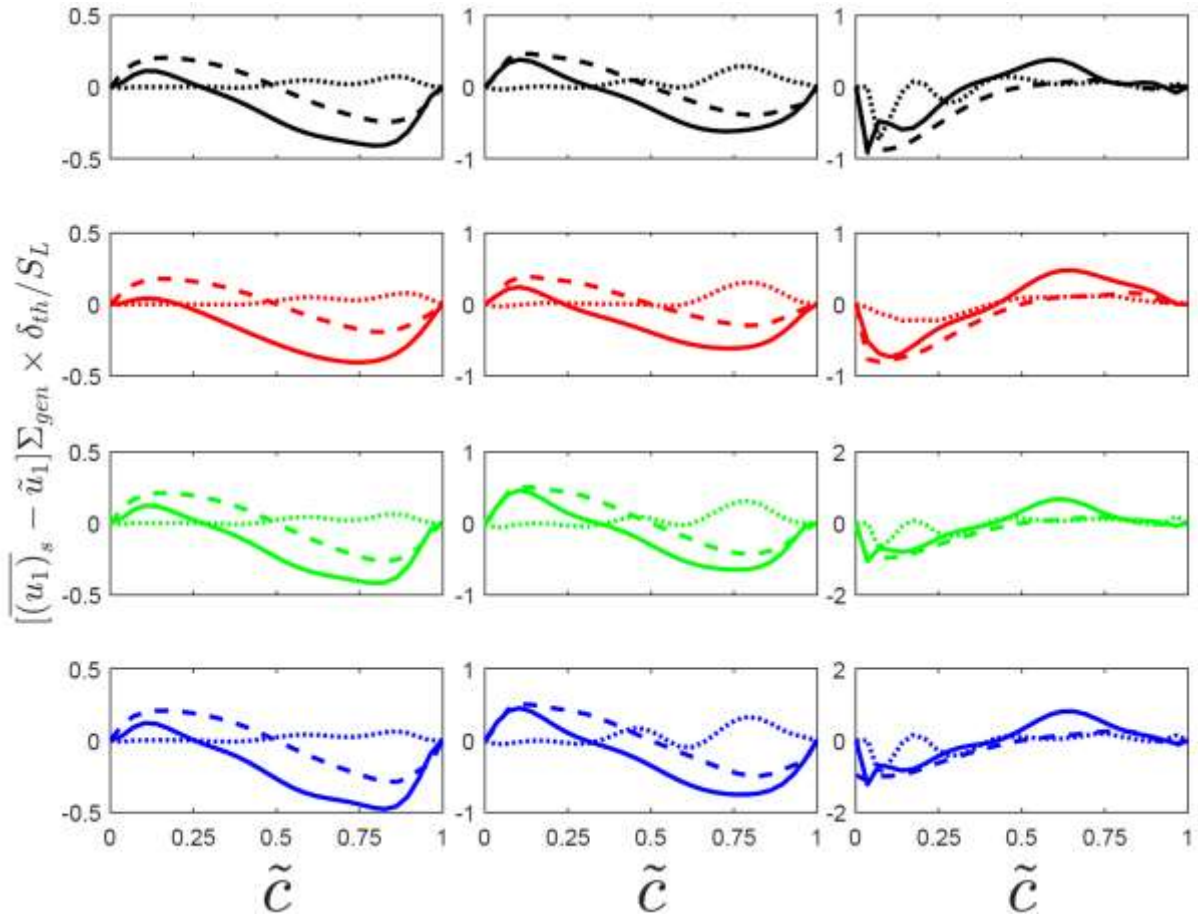

Fig. 2: Variation of $\left[\overline{(u_i)}_s - \tilde{u}_i\right]\Sigma_{\text{gen}} \times \delta_{th}/S_L$ (solid lines for DNS data) along with the predictions of the gradient hypothesis (dotted line) and eq. 3 (broken line) with $\tilde{c}$ for cases A-C from left to right columns respectively.

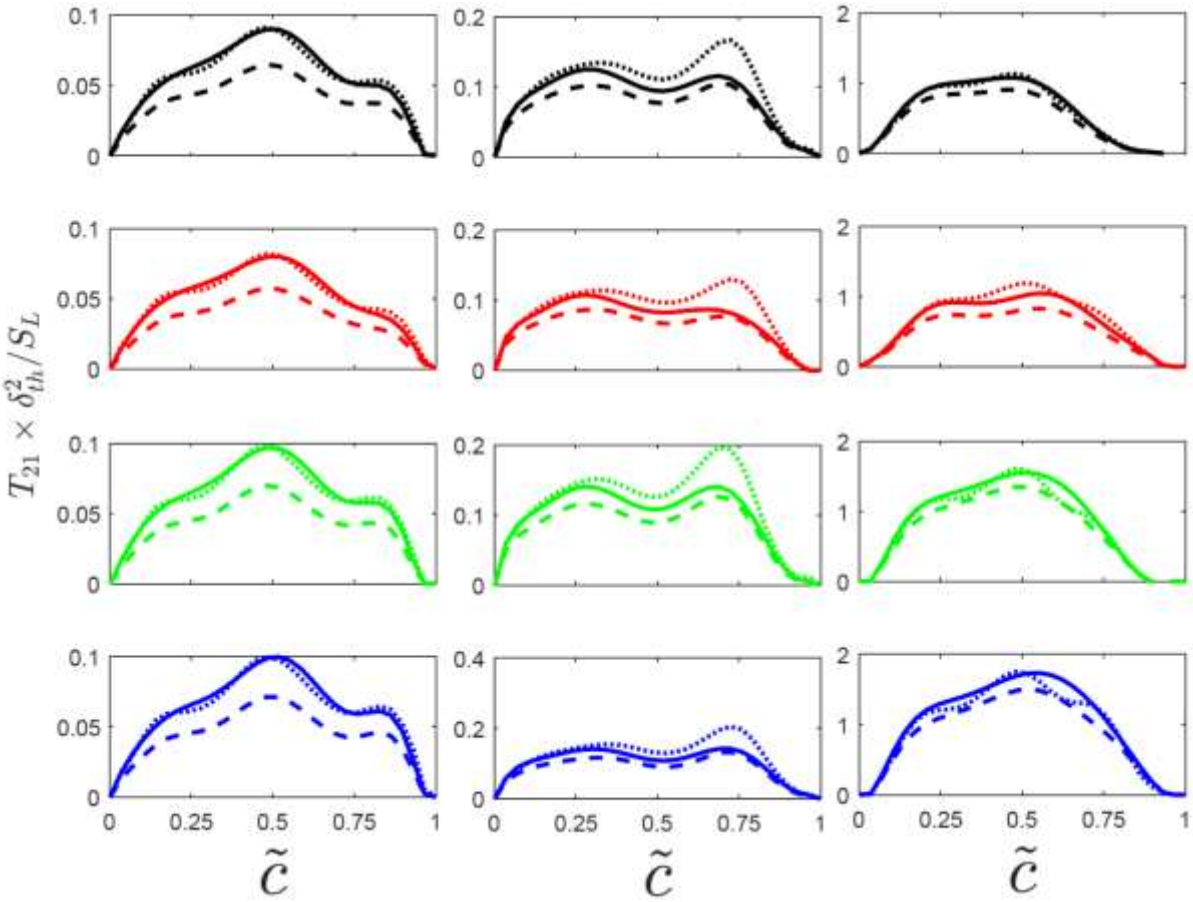

Fig. 3: Variation of $T_{21} \times \delta_{th}^2/S_L$ (solid lines for DNS data) along with the predictions of the CPB (broken line) and VPDM (dotted line) models with $\tilde{c}$ for cases A-C from left to right columns respectively.

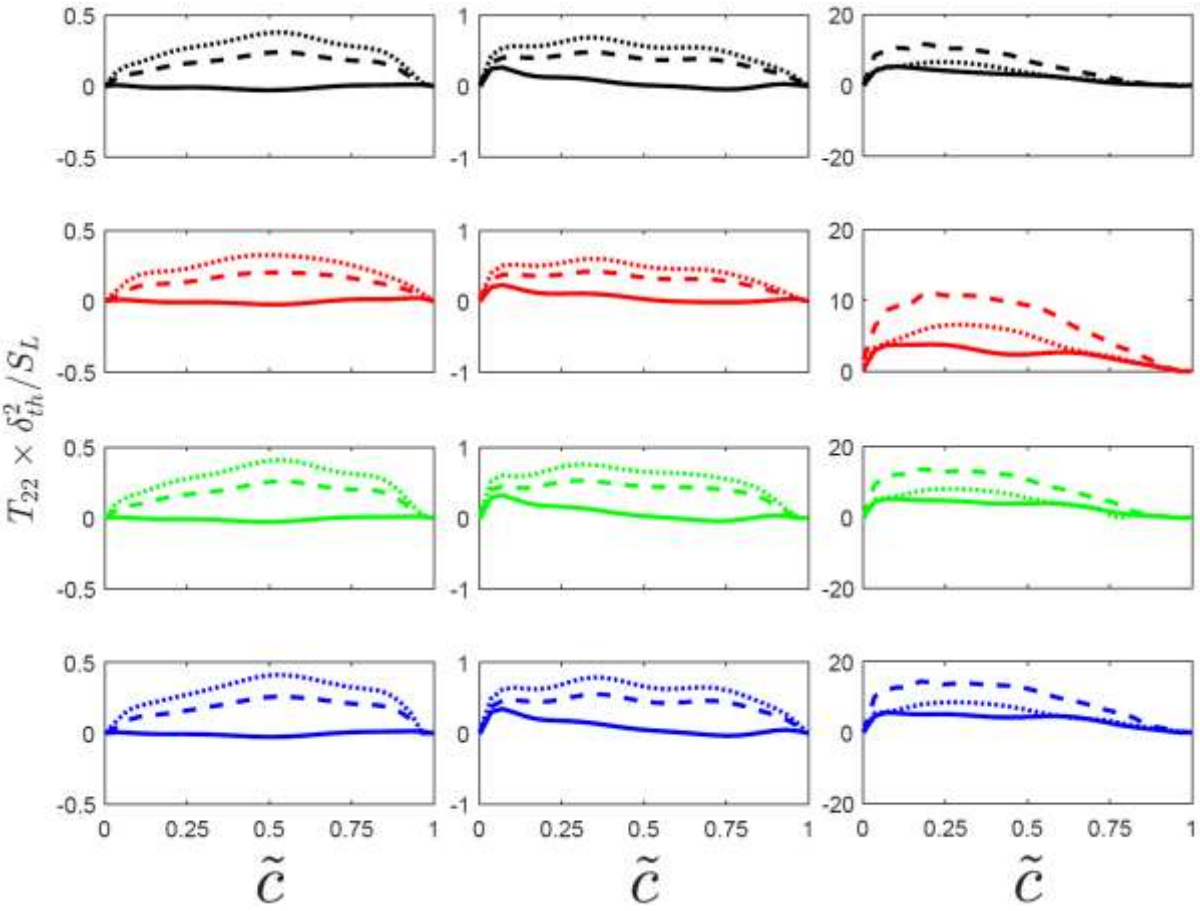

Fig. 4: Variation of $T_{22} \times \delta_{th}^2/S_L$ (solid lines for DNS data) along with the predictions of the CPB (broken line) and CFM (dotted line) models with $\tilde{c}$ for cases A-C from left to right columns respectively.

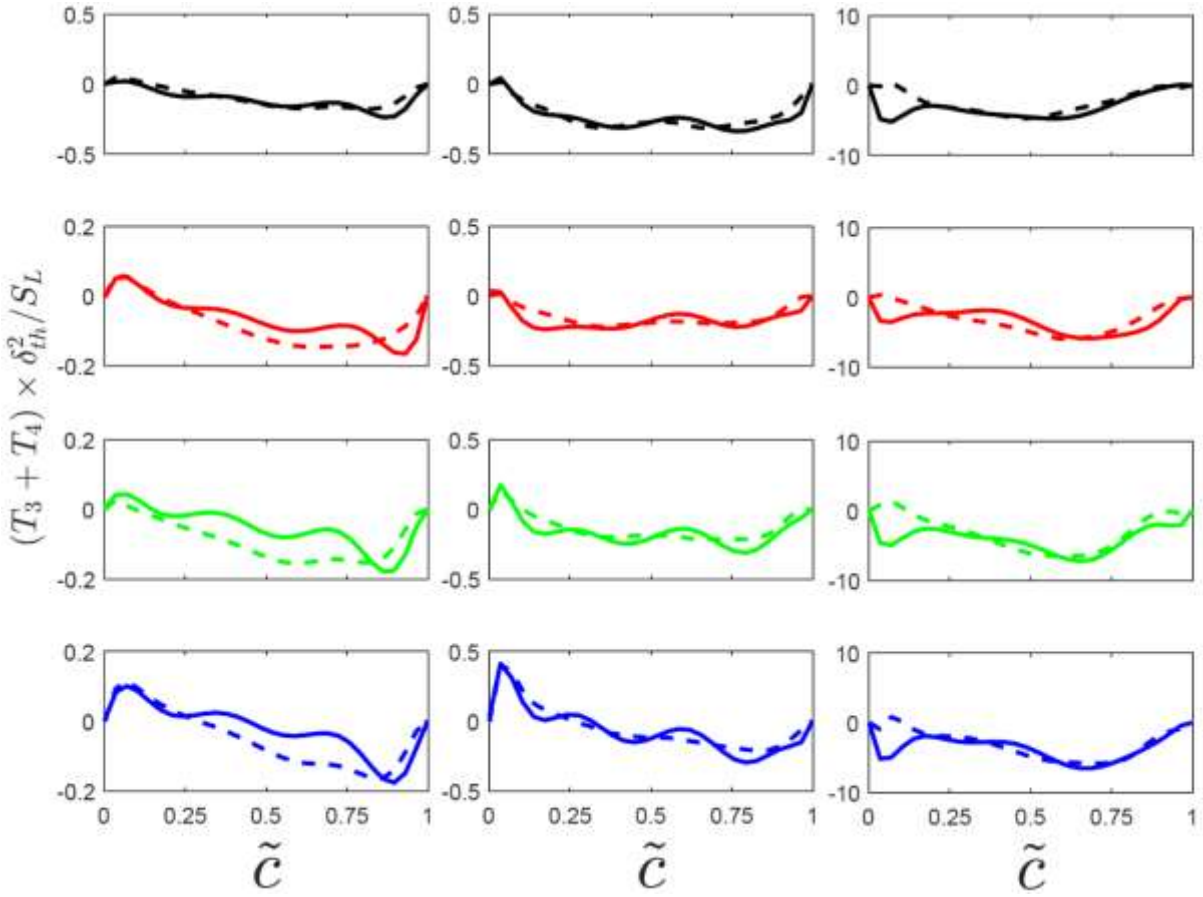

Fig. 5: Variation of $(T_3 + T_4) \times \delta_{th}^2 / S_L$ (solid lines for DNS data) along with the predictions of eq. 5 with β_0 given in Table 2 (broken line) with $\tilde{c}$ for cases A-C from left to right columns respectively.

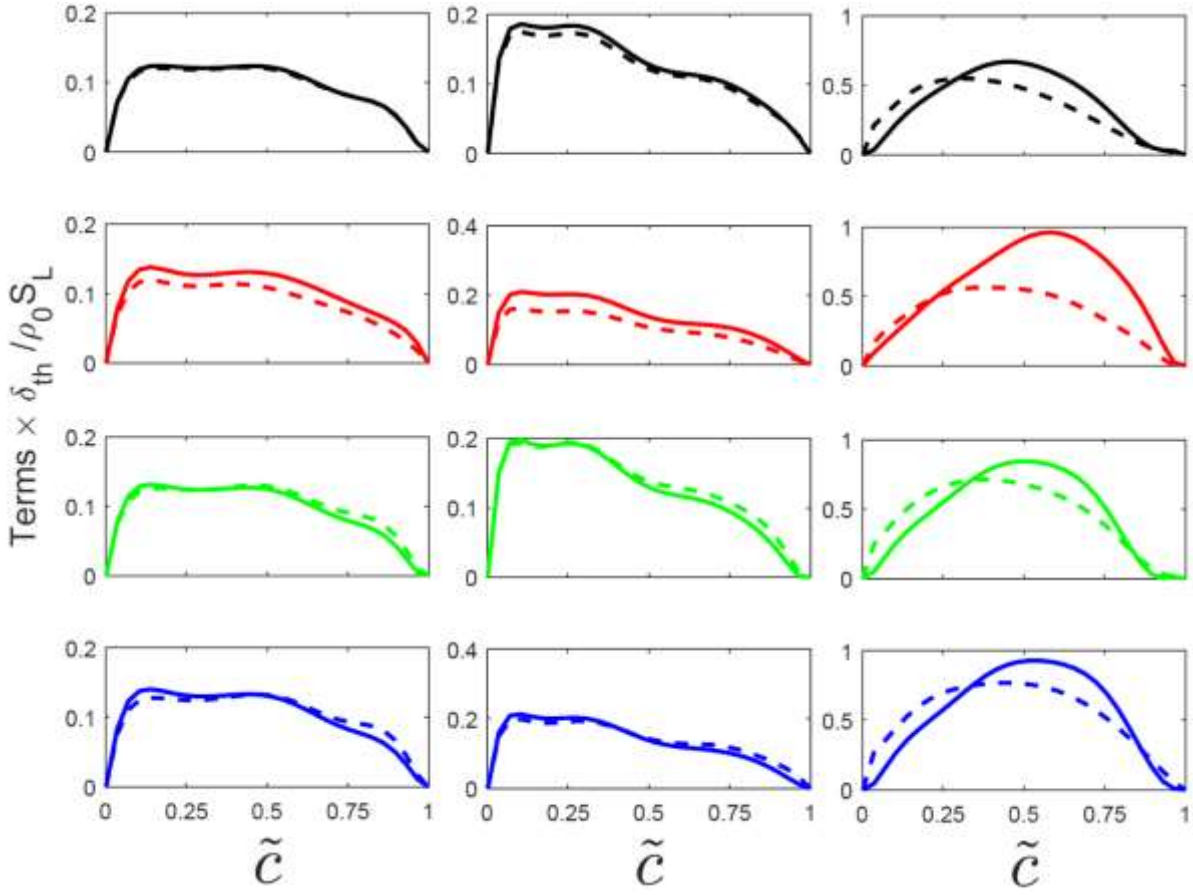

Fig. 6: Variations of $\bar{\dot{w}} \times \delta_{th}/\rho_0 S_L$ (solid line), along with $\rho_0 S_L \Sigma_{gen} \times \delta_{th}/\rho_0 S_L$ (broken line) with $\tilde{c}$ for cases A-C from left to right columns respectively.